scientific reports

OPEN

Frost heave cracking and uniaxial compression failure behavior of sandstone samples containing a flaw filled with water

Duofeng Cen[1✉] & Yage Li[2]

The frost heave failure mechanism of fractured rock mass is a complicated problem faced by engineering construction in cold area. In this study, low temperature frost heave test and post-freezing uniaxial compression test on sandstone samples with a water-filled flaw were carried out. The frost heave cracking mode, frost heave pressure, frost heave cracking criterion and the effect of frost heave-induced cracks on post-freezing uniaxial compression failure behavior under different flaw inclination angles (0~90°) and freezing temperatures (−10~−40 °C) were investigated. Frost heave cracks initiate and extend along the coplanar direction of flaws. The frost heave damage degree decreases with the increase of flaw inclination angle. As the freezing temperature drops, the flaw cracking length first increases greatly, and then decreases, reaching the maximum at −15 °C. The evolution of frost heave pressure can be divided into six stages: pre-freeze stage, rapid increase stage, rapid decrease stage, stable stage, slight rebound stage and dissipation stage. The peak frost heave pressure first increases and then decreases with the increase of flaw inclination angle, and reaches the maximum at 60°, and increases as the freezing temperature drops. Formulas for calculating the critical stress intensity factor K_{IC} for flaw frost heave cracking are provided, considering flaw inclination angle or freezing temperature. When the flaw is within a certain range of inclination angles (45~75°), cracks under uniaxial compression will extend from the frost heave-induced cracks.

If the temperature of water in the rock flaws reaches the freezing point or below, the water–ice phase transition will occur, resulting in frost heave pressure. When the frost heave pressure exceeds the rock strength, frost heave damage and cracking of flaws will occur, thus affecting the mechanical properties and stability of rock masses[1–4]. Exploring the frost heave damage and cracking mechanism of water-filled rock masses under low temperature and its influence on rock mass mechanical properties can provide theoretical reference for the safety evaluation of rock engineering construction in cold area.

Understanding the frost heave pressure characteristics of water-filled flaws under low temperature is the key to understanding the frost heave cracking mechanism of flaws[5,6]. Winkler[7] conducted water–ice phase transition tests at different temperatures and found that if the pore volume of rock remained unchanged, the frost heave pressures at −5 °C, −10 °C and −20 °C reached 61.0, 133.0 and 211.5 MPa, respectively. Davidson and Nye[8] applied photoelastic effect to measure the pressure caused by freezing expansion of transparent materials, founding that the maximum frost heave pressure in the saturated flaw with a width of 1 mm was 1.1 MPa. Arosio et al.[9] measured that the maximum frost heave pressure in the saturated flaw with a width of 4 mm reached 5 MPa by using the thin film pressure sensor. Huang et al.[10] measured that the maximum frost heave pressure in water-filled flaws exceeded 4 MPa. The maximum frost heave pressure measured by Lin et al.[11] was 6.98 MPa. It can be seen that the frost heave pressure presented by different researchers is very different. The main reason is that there are many factors affecting frost heave pressure, which are related to flaw geometry, unfrozen water content, freezing rate, flaw saturation and physical and mechanical properties of rock. Some researchers have analyzed the mechanism of frost heave pressure generation in flaws and frost heave cracking. Michaud and Dyke[1] believed that the water pressure of frost heave in flaws was determined by the freezing rate. Liu et al.[12] and McGreevy and Whalley[13] clarified that high head pressure caused by water–ice phase transition

[1]Institute of Rock Mechanics, Ningbo University, Ningbo 315211, China. [2]School of Civil and Transportation Engineering, Hebei University of Technology, Tianjin 300401, China. ✉email: cdfschool@126.com

during frost heave is the fundamental cause of tensile failure of defects in rock masses. However, Derjaguin and Churaev[14] and Churaev and Sobolev[15] indicated that the separation pressure on the unfrozen water film is the cause of frost heaving in the pore medium. When the separation pressure exceeds the pressure that the pore skeleton can bear, the pore will fracture. Vlahou and Worster[16] presented that the increase in water pressure during the early freezing stage can lead to the fracturing of cavities. Walder and Hallet[17] proposed that frost heave cracking of flaws was caused by volume water migrating to flaws and freezing. Tan et al.[18,19] and Murton et al.[20,21] quantitatively investigated the influence of water migration on rock fracture at freezing temperature. Liu et al.[22] explained the frost heave damage mechanism of fractured rock under freeze–thaw cycle from the perspective of fracture mechanics. Jia et al.[23] and Lv et al.[24] measured the deformation and temperature change of flaws during freezing test. Tharp[25] suggested that flaws with a length-to-width ratio greater than 0.01 were prone to frost heave cracking, and proposed a calculation method of frost heave cracking stress intensity factor.

Low temperature freezing will affect the mechanical properties of fractured rock masses. Jia et al.[26] and Liu et al.[27] carried out uniaxial compression tests on sandstone samples containing three ice-filled *en-echelon* flaws in combination with high-speed imaging and acoustic emission technique, and found that due to the supporting and adhesive actions of ice in rock pores and flaws, ice filling strengthened the samples. The flaw inclination angle and freezing temperature have great influence on the crack propagation behavior. Wang et al.[28] performed Brazilian splitting test on marble disc samples with double ice-filled flaws, and observed that the tensile strength was higher than that of the unfilled samples, and the filling and adhesive actions of ice controlled the tensile strength and crack propagation behavior. Bai et al.[29] conducted triaxial compression tests on cylindrical sandstone samples containing two ice-filled open flaws to study the strength, deformation and crack propagation behavior combined with acoustic emission detection. Huang et al.[10,30] investigated the cracking behavior of similar material samples with single and double flaws and the loss of uniaxial compression strength under freeze–thaw cycles. Shan et al.[31] carried out triaxial unloading creep tests of single-flaw red sandstone filled with ice, and established a creep damage model. Zhu et al.[32] studied the dynamic cracking mechanism of ice-filled single-flaw sandstone by drop weight tests, and analyzed the influence of flaw inclination and length. The above research shows that when flaws are filled with ice, the strength of rock masses may be improved due to the supporting and adhesive actions of ice, but the strength of the damaged rock masses after freezing and thawing will be reduced.

The above studies have provided a certain understanding of the frost heave pressure, strength and failure mechanism of water-filled rock masses under low temperature freezing. Nevertheless, research in this area remains limited. In particular, the effect of frost heave-induced cracks on the uniaxial compressive failure behavior requires further investigation. In view of this, low temperature frost heave test and uniaxial compression test after frost heave on sandstone samples with a perforated flaw filled with water were designed and carried out in this study, and the flaw frost heave cracking mode, frost heave pressure, frost heave cracking criterion and the effect of frost heave-induced cracks on uniaxial compression failure behavior under different flaw inclination angles and freezing temperatures were investigated.

Test methods
Sample preparation
Red sandstone, which is common and easy to ensure uniformity, was selected as the research object, and the samples were cut and processed from a complete stone to reduce the discreteness of the test results. The physical and mechanical parameters of the rock is listed in Table 1. As shown in Fig. 1, the size of the sandstone cube sample is 100 mm × 50 mm × 50 mm. A flaw with a length of 15 mm, a width of 3 mm and a depth of 50 mm was processed in the middle of the sample by a fine carving machine. The flaw penetrates the sample. The flaw inclination angle (the angle between the sample cross-section and flaw) α was set to 0°, 15°, 30°, 45°, 60°, 75° and 90°, respectively. The single-flaw sandstone samples with different inclination angles after processing are shown in Fig. 2.

Test schemes
Frost heave test scheme
The temperature control test chamber was used to carry out the frost heave test of single-flaw sandstone samples at low temperature. The temperature of the test chamber can be adjusted from −40 °C to 130 °C, which can meet the requirements of the low temperature scheme of the test. Flexiforce, a thin film pressure sensor, was used to monitor frost heave pressure in rock flaws. The standard Flexiforce sensor (Model: A201) is available with a range of 0 ~ 100 lbs, a maximum force of 440 lbs, a circular sensing area with a diameter of 9.53 mm and a thickness of 0.208 mm. The sensor was calibrated before the test. The data acquisition system of the thin film pressure sensor was used to collect the output pressure value of the sensor. The test device is shown in Fig. 3.

Waterproof glue was used to seal the openings at both ends of the flaw in order to inject water into the flaw and prevent water loss. At the same time, the thin film pressure sensor was passed through the waterproof glue at one end of the flaw and preset into the flaw with a depth of 25 mm, so that the sensor sensing area was located in the middle of the flaw. After the glue was solidified, a fine needle syringe was used to fill the flaw with water, and the sample was placed in pure water for 72 h and finally no bubbles were generated. Since a

Density (g/cm³)	Uniaxial compressive strength (MPa)	Uniaxial tensile strength (MPa)	Elasticity modulus (GPa)
2.26	47.73	2.96	3.37

Table 1. Physical and mechanical parameters of the red sandstone.
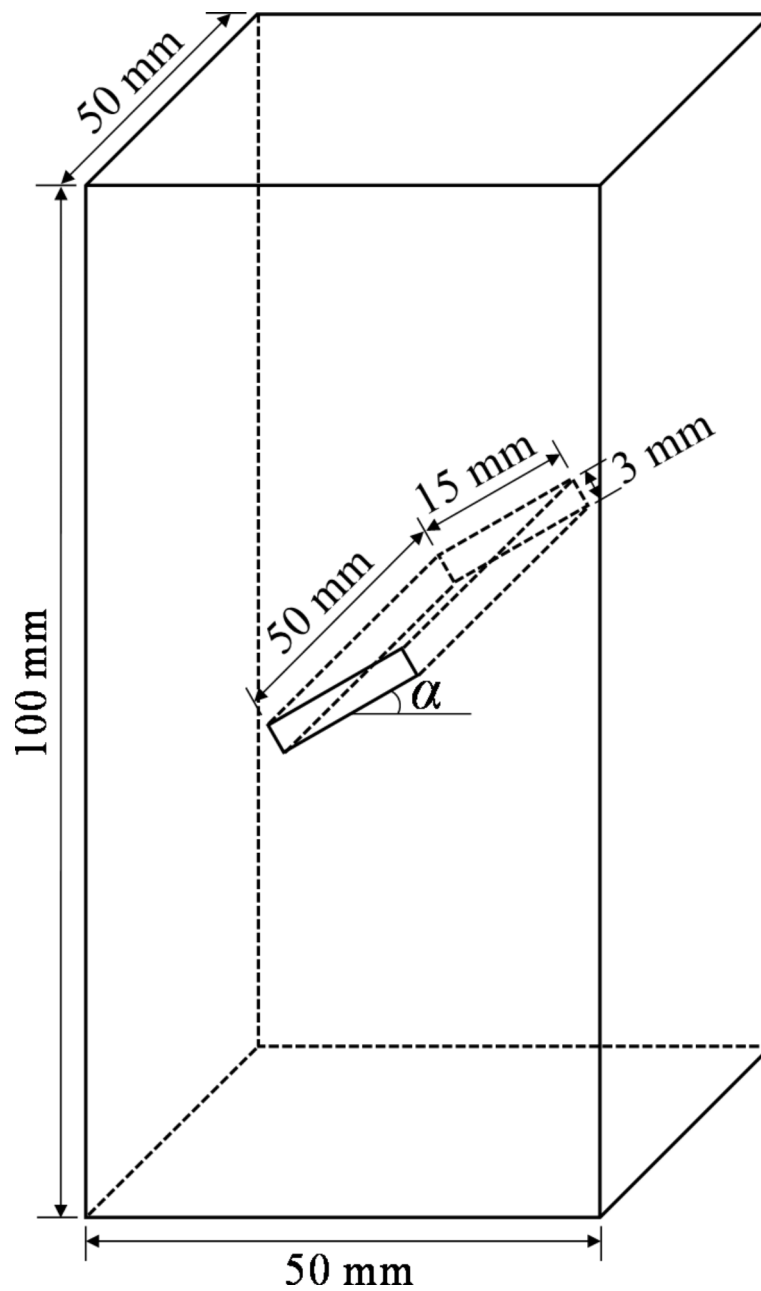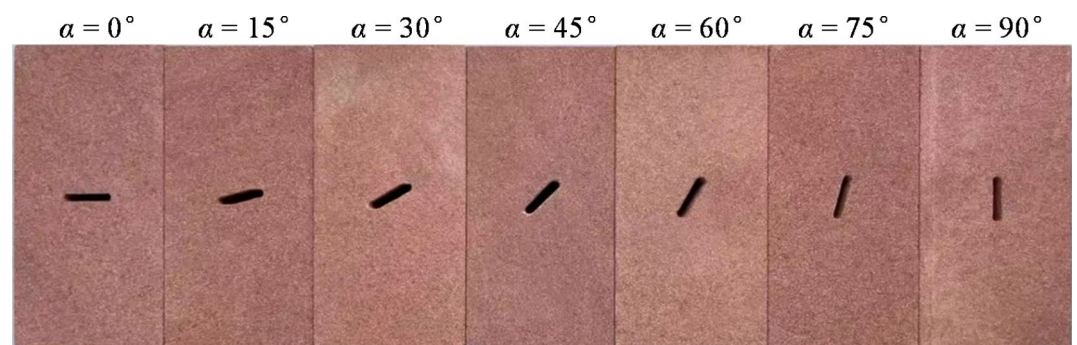
Fig. 1. Sample geometry.
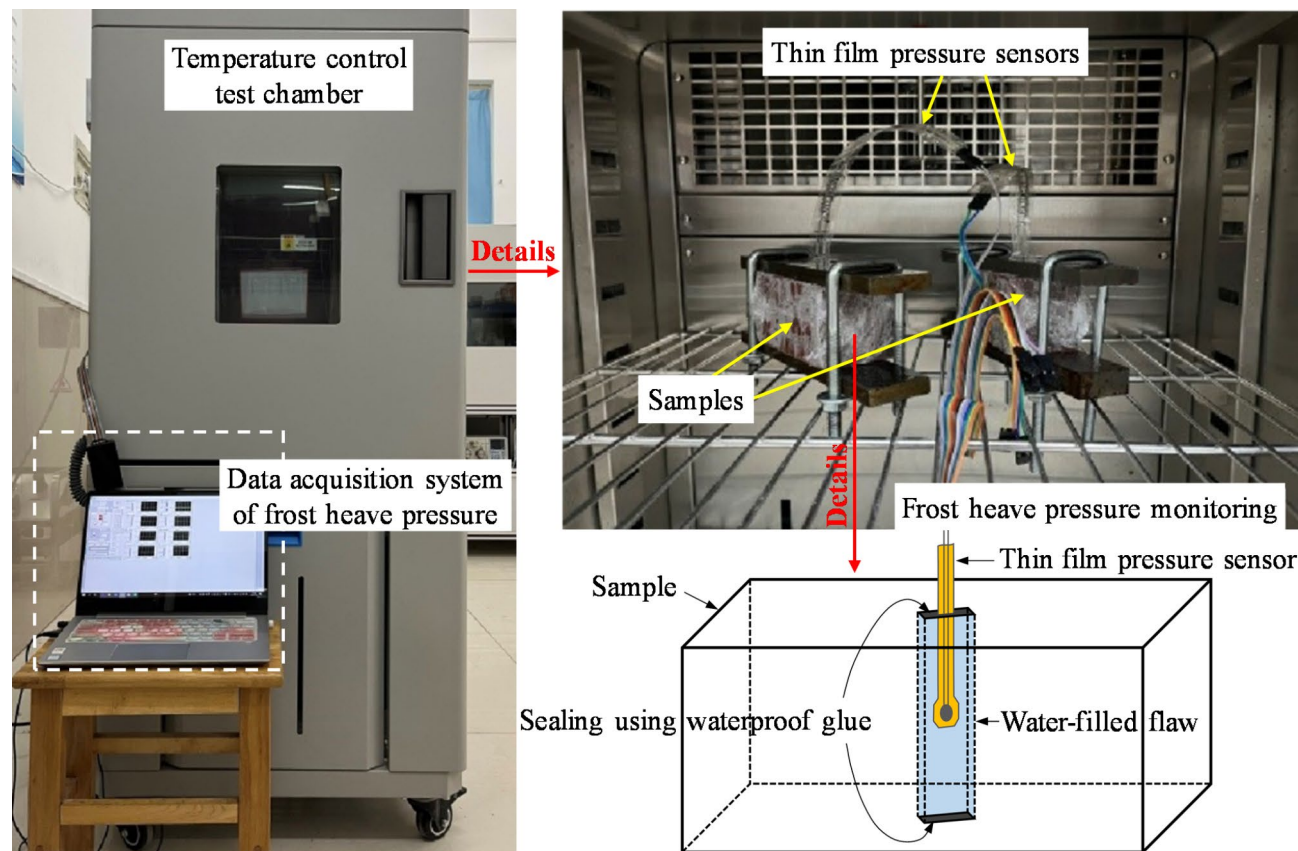

Fig. 2. Single-flaw sandstone samples.

Fig. 3. Frost heave test device.

Test scheme	Flaw inclination angle α (°)	Freezing temperature T (°C)
Under different flaw inclination angles	0	-20
	15	-20
	30	-20
	45	-20
	60	-20
	75	-20
	90	-20
Under different freezing temperatures	30	-10
	30	-15
	30	-20
	30	-30
	30	-40

Table 2. Frost heave test scheme.

small amount of water in the flaw will be absorbed by the rock before the sample was fully moistened, the water filling state of the flaw was often checked during the soaking process, and timely water replenishment was required to make the flaw full of water. Frost heave test was carried out after the sample was fully soaked. Set the temperature control test chamber to the predetermined freezing temperature, reduce from normal temperature to the predetermined freezing temperature at a certain rate (about 1 °C/min) and maintain a certain time (about 5 h) at the predetermined temperature, and then rise to normal temperature, the frost heaving test process was completed. Frost heave tests under different flaw inclination angles and freezing temperatures were carried out to explore the frost heave cracking of flaws and the variation of frost heave pressure. The specific frost heave test scheme is shown in Table 2.

Uniaxial compression test scheme after frost heave

The electrohydraulic servo testing machine WAW-300 was used to conduct uniaxial compression test at room temperature on the single-flaw sandstone samples after frost heave cracking, and to explore the compression mechanical behavior after frost heave. A displacement control method of 0.1 mm /min was used to load the melted samples after frost heave.

Frost heave test results
Frost heave cracking mode of flaw

In order to explore the frost heave cracking mode of flaws, samples with different flaw inclination angles at −20 °C were selected for analysis. The flaw frost heave cracking photos and sketch are shown in Fig. 4. The frost heave-induced cracks coplanar with the flaw initiated at the flaw tips when the flaw inclination angle is 0°, and the cracks extended to the edges of the sample. The cracks initiated at the flaw tips when the flaw inclination angle is 15°, but the right crack of the flaw extended approximately horizontally and to the edge of the sample. Frost heave-induced cracks extended along the coplanar direction of flaws at 30 ~ 90° inclination angles; however, at 75° and 90° inclination angles, there were only short cracks at the tips of the flaws. It can be seen that cracks initiate and extend along the coplanar direction of flaws under the action of frost heave in general, but the frost heave damage degree of flaws with different inclination angles is different. The flaw of 0° inclination angle has the most severe frost heave damage and the longest cracking, the flaws of 30°, 45° and 60° inclination angles have the second frost heave damage, and the flaws of 75° and 90° inclination angles have the least frost heave damage. This is mainly because when the flaw inclination angle is smaller, the flaw trend is closer to the width direction of the sample, and the width of the sample is smaller than the length, so the flaw is more prone to frost heave cracking.

Figure 5 shows the variation of crack propagation length (the total length of the cracks at both ends of the flaw) with freezing temperature (taking 30° flaw inclination angle as an example). With the decrease of freezing temperature, the crack propagation length first increases greatly, and then decreases slightly (except the circumstance of −30 °C, which may be caused by the discreteness of the test results), reaching the maximum at −15 °C. This may be because the frost heaving pressure of ice does not increase indefinitely with the drop of freezing temperature.

Frost heave pressure in flaw
Evolution of frost heave pressure

Sample with freezing temperature of −10 °C and flaw inclination angle of 30° is selected as an example to analyze the frost heave pressure curve, as shown in Fig. 6. The evolution of frost heave pressure can be divided into the following six stages:

Pre-freezing stage (OA): When the temperature is above 0 °C, there is no water–ice phase transition in the flaw, and the frost heave pressure is always zero.

Rapid increase stage (AB): Once the temperature in the flaw reaches the freezing point of water at 0 °C, the water–ice phase transition occurs in the flaw, and the resulting frost heave pressure reaches its peak in just a few minutes (about 5 MPa in Fig. 6).

Rapid decrease stage (BC): In this stage, the frost heave pressure drops sharply. This is because when the frost heave pressure generated in the flaw makes the flaw tip stress reach the cracking strength, cracking occurs at the flaw tips, and the frost heave pressure falls rapidly from the peak to a certain value (below 1 MPa in Fig. 6).

Stable stage (CD): As the freezing temperature remains constant, the frost heave pressure in the flaw also tends to stabilize with little change.

Slight rebound stage (DE): This stage is the temperature rise stage in the later stage of the test. With the increase of temperature, the frost heave pressure will rise again and reach a second peak. This is because when the temperature rises, the cold shrinkage deformation generated by the rock matrix under the action of low temperature will gradually rebound, so that the flaw faces produce a certain extrusion to the ice, resulting in a small recovery of frost heave pressure.
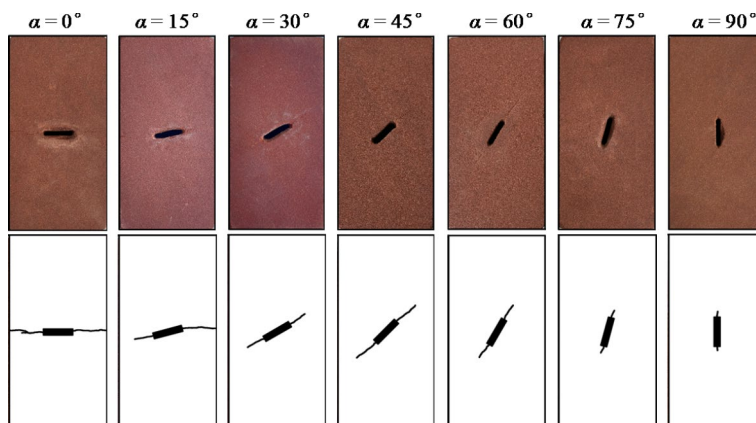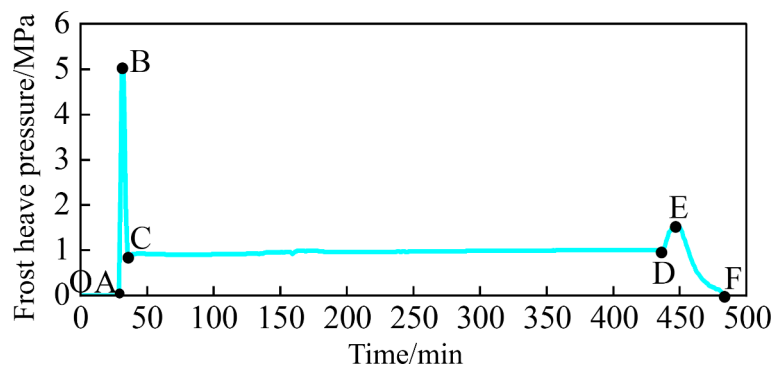

Fig. 4. Flaw frost heave cracking ($T = -20$ °C).
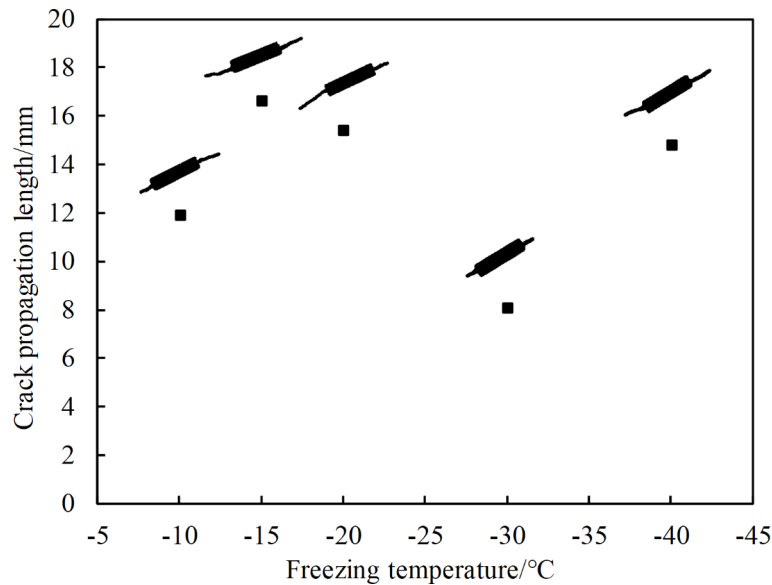
Fig. 5. Variation of crack propagation length with freezing temperature ($\alpha = 30°$).

Fig. 6. Evolution of flaw frost heave pressure ($\alpha = 30°$, $T = -10$ °C).

Dissipation stage (EF): When the temperature rises above 0 °C, the ice in the flaw begins to melt, the frost heave pressure gradually decreases, and finally dissipates.

Effect of flaw inclination angle on frost heave pressure
Figure 7 shows the peak frost heaving pressures in the flaws with different inclination angles, taking −20 °C freezing temperature as an example. The peak frost heave pressure first increases and then decreases with the increase of flaw inclination angle, and reaches the maximum when the flaw inclination angle is 60°. Specifically, from the inclination angle of 0° to 60°, the peak frost heave pressure gradually increases from 5.55 MPa to 7.45 MPa, an increase of 34.23%. From the inclination angle of 60° to 90°, the peak frost heave pressure decreases significantly from 7.45 MPa to 3.94 MPa, decreasing 47.11%, and the peak frost heave pressures corresponding to the inclination angles of 75° and 90° are smaller than that corresponding to the inclination angle of 0°, and the peak frost heave pressure is the smallest at the inclination angle of 90°. This phenomenon is primarily because as the flaw inclination angle increases, the orientation of the flaw becomes increasingly aligned with the length direction of the sample, necessitating a greater frost heave pressure to induce cracking. While at inclination angles of 75° and 90°, the flaws encounter difficulties in propagation, leading to a certain degree of spalling around the flaws, which results in an inability to withstand greater frost heave pressure.

Effect of freezing temperature on frost heave pressure
Figure 8 presents the peak frost heave pressures in the flaws at different freezing temperatures, taking the flaw with 30° inclination angle as an example. In general, the peak frost heave pressure increases with the drop of freezing temperature. Especially when the temperature drops from −10 °C to −15 °C, the peak frost heave pressure increases relatively quickly, from 5.03 MPa to 6.55 MPa, with a growth rate of 0.3 MPa/°C. When the temperature drops from −15 °C to −40 °C, the peak frost heave pressure increases relatively slowly, from 6.55 MPa to 7.88 MPa, with a growth rate of 0.05 MPa/°C. The reason for the increase in peak frost heave

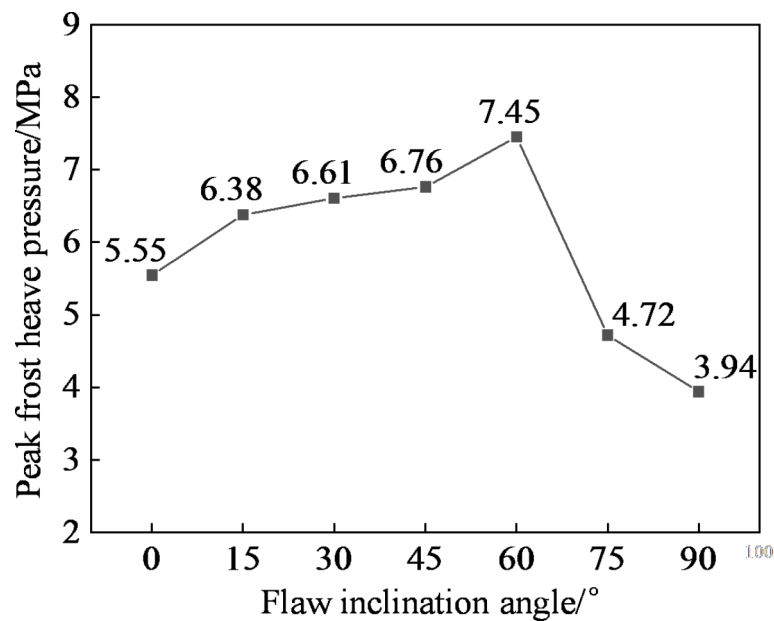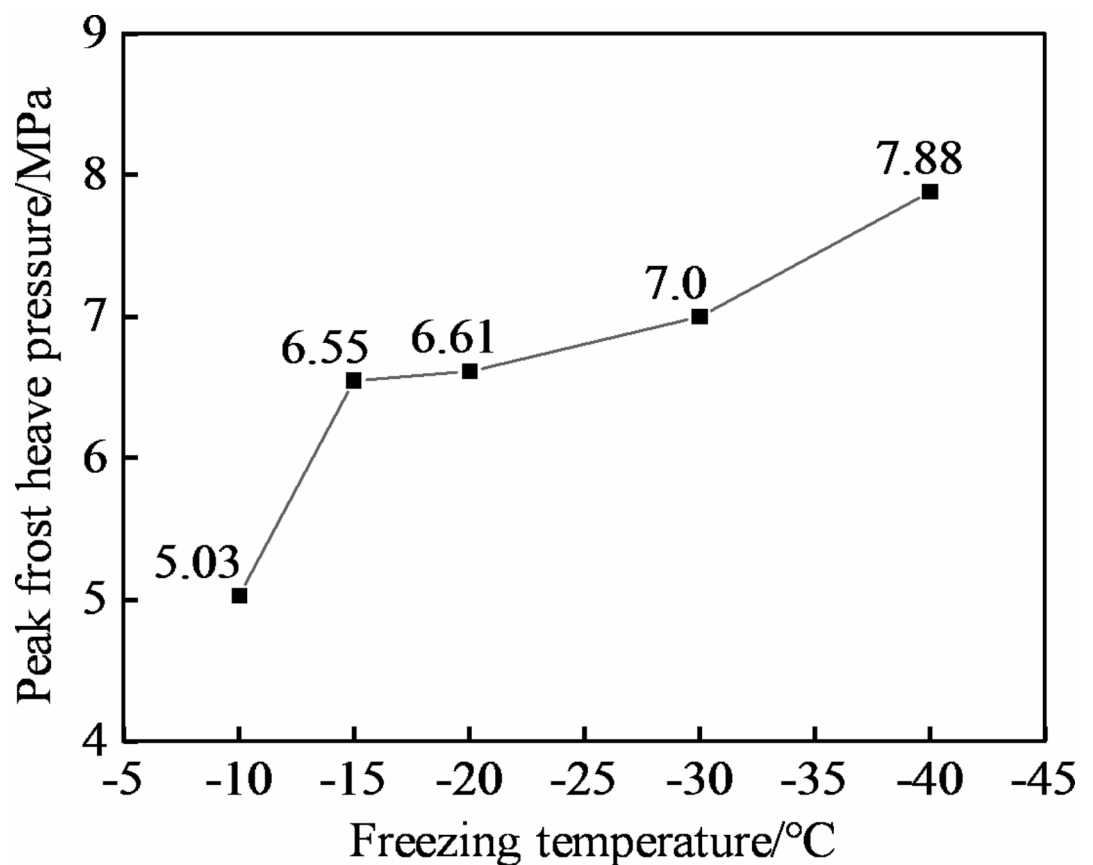**Fig. 7**. Peak frost heaving pressures in the flaws with different inclination angles ($T = -20\ °C$).

Fig. 8. Peak frost heave pressures in the flaws at different freezing temperatures ($\alpha = 30°$).

pressure may be attributed to that lower freezing temperature enhances the ice cementation strength in the pores of unsaturated rocks. This, in turn, leads to an increase in rock strength, necessitating a greater frost heave pressure to induce cracking of the flaw. However, due to the limited cementation strength of ice, the increase rate of peak frost heave pressure significantly decreases when the freezing temperature falls below $-15\ °C$. For

the same reason, although the frost heave pressure at a freezing temperature below − 40 °C was not tested in this study, it can be inferred that as the freezing temperature continues to decrease, the increase rate of peak frost heave pressure will gradually diminish.

Frost heave cracking criterion

The frost heave pressure causes crack I (open type) fracture. The critical stress intensity factor K_{IC} can be calculated according to fracture mechanics theory, and the frost heave cracking criterion of flaws can be established. The flaw is simplified as an elliptical flaw, and the calculation unit of stress field near the flaw tip is shown in Fig. 9. The polar coordinate expression of each stress component near the flaw tip under frost heave is as follows:

$$\sigma_{ij} = \frac{K_I}{\sqrt{2\pi r}} f_{ij}(\theta) \tag{1}$$

The $f_{ij}(\theta)$ in Eq. (1) is calculated as follows:

$$\begin{cases} f_{xx}(\theta) = cos\frac{\theta}{2}\left(1 - sin\frac{\theta}{2}sin\frac{3\theta}{2}\right) \\ f_{yy}(\theta) = cos\frac{\theta}{2}\left(1 + sin\frac{\theta}{2}sin\frac{3\theta}{2}\right) \\ f_{xy}(\theta) = cos\frac{\theta}{2}sin\frac{\theta}{2}\cos\frac{3\theta}{2} \end{cases} \tag{2}$$
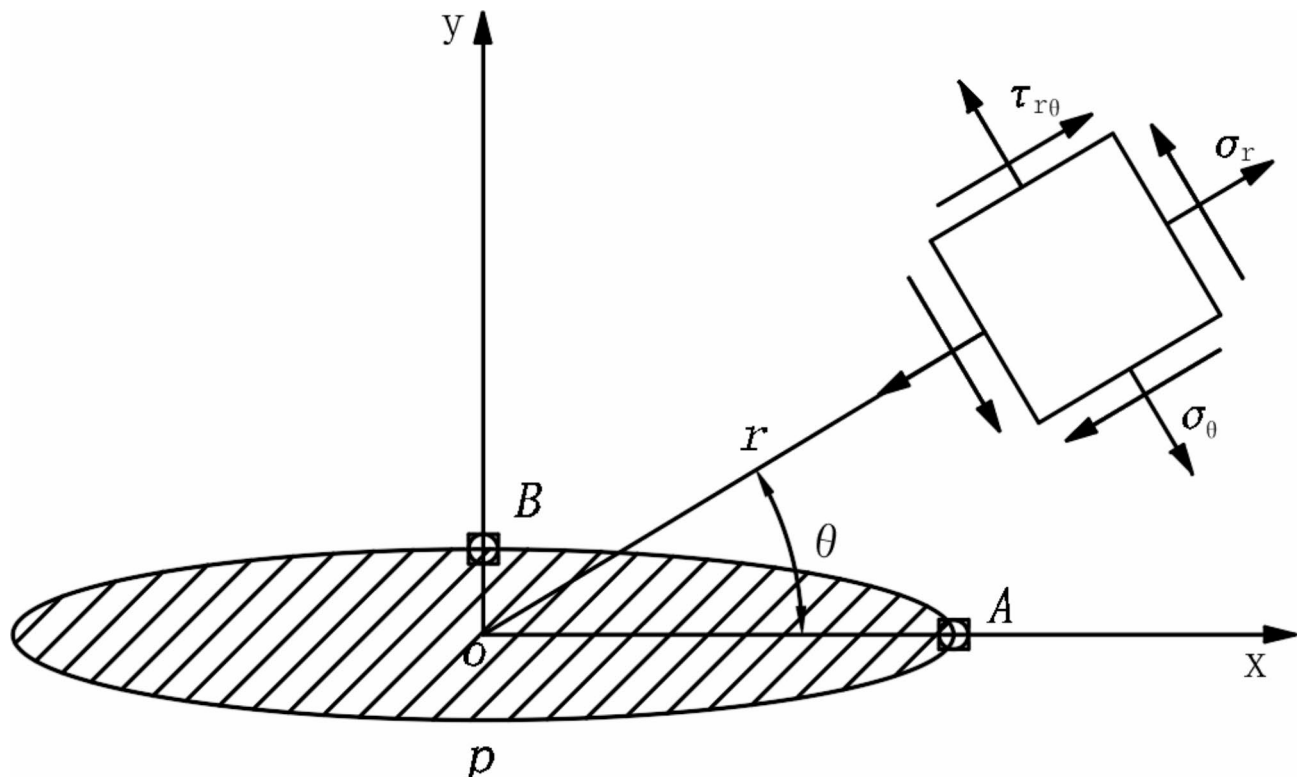
where K_I is the stress intensity factor of type I crack.

According to the theory of fracture mechanics, the theoretical analytic solution expression of the stress component of the flaw end perpendicular to the flaw surface is as follows:

$$\sigma_{zz}(x,0) = \begin{cases} -p(|x| \leqslant a) \\ \dfrac{p\,|x|}{\sqrt{x^2 - a^2}} - p(|x| > a) \end{cases} \tag{3}$$

where p is frost heave pressure, and a is half of the flaw length.

According to the solution method of stress intensity factor for type I crack, the stress intensity factor K_I under frost heave pressure is calculated as follows:

Fig. 9. Calculation model of stress field near the flaw tip (after Huang et al.[33]).

$$K_I = \lim_{x \to a+} \sqrt{2\pi(x-a)}\sigma_{zz}(x,0) \tag{4}$$

Assuming that frost heave pressure p uniformly acts on the flaw surface, then the stress intensity factor of the flaw is:

$$K_I = \frac{1}{\sqrt{2\pi a}}\int_{-a}^{a}\sigma_{zz}(x,0)\left(\frac{a+x}{a-x}\right)^{\frac{1}{2}}\mathrm{d}x = \frac{p}{\sqrt{2\pi a}}\int_{-a}^{a}\left(\frac{a+x}{a-x}\right)^{\frac{1}{2}}\mathrm{d}x = p\sqrt{\pi a} \tag{5}$$

When the stress intensity factor K_I of flaw is greater than the critical stress intensity factor K_{IC}, cracking occurs.

The peak frost heave pressure of flaw is regarded as the frost heave pressure of crack initiation, that is, the critical frost heave stress of cracking. The peak frost heave pressures at different flaw inclination angles and freezing temperatures obtained by the above tests were substituted into Eq. (5) to obtain the critical stress intensity factors K_{IC} at different flaw inclination angles and freezing temperatures, as displayed in Fig. 10.

As shown in Fig. 10, the calculated critical stress intensity factors were fitted to obtain the frost heave cracking criterion of flaws, considering the flaw inclination angle or freezing temperature. The fitting expression considering different flaw inclination angle is as follows:

$$K_{IC} = 0.847 + 0.009\alpha - 7.307 \times 10^{-5}\alpha^2 - 7.407 \times 10^{-7}\alpha^3 \tag{6}$$

The application range of the flaw inclination angle is $0° \leq \alpha \leq 90°$, and the freezing temperature is -20 °C.

The fitting expression considering different freezing temperatures is as follows:

$$K_{IC} = -0.139 - 0.138T - 0.005T^2 - 6.570 \times 10^{-5}T^3 \tag{7}$$

The application range of the freezing temperature is -40 °C $\leq T \leq -10$ °C, and the flaw inclination angle is 30°.

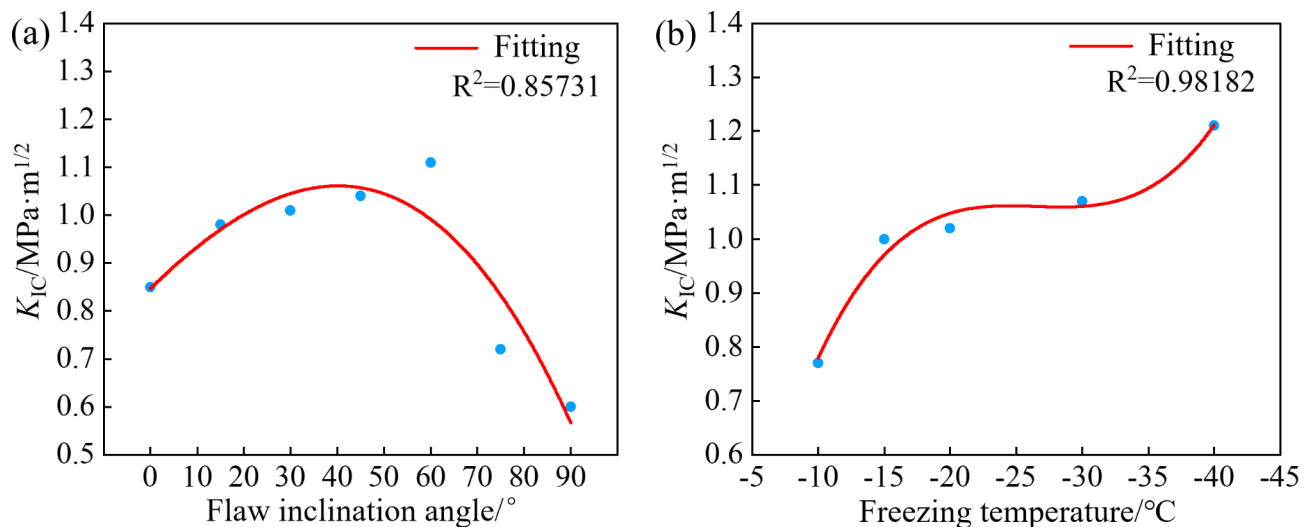## Uniaxial compression test results after frost heave cracking
### Deformation and strength characteristics
Stress–strain curve
Figure 11 shows the stress–strain curves of melted single-flaw sandstone samples obtained by uniaxial compression test at room temperature after frost heave cracking. As shown in Fig. 11a, the stress–strain curves can be divided into the following four stages:

Compaction stage (OA): During the initial compression process, original pores, prefabricated flaw and frost heave-induced cracks in the sample are closed, the particle structure inside the sample becomes more dense, the curve is concave, and the tangent modulus gradually increases. The curve shapes and lengths of different samples at this stage are different due to different flaw inclination angles and frost heave damage degrees.

Elastic deformation stage (AB): At this stage, the stress–strain basically increases linearly, and the sample exhibits approximate linear elasticity. The elastic modulus varies with the flaw inclination angle and freezing temperature. In general, the elastic modulus is maximum at 60° inclination angle, smaller at 75° and 90° inclination angles, and decreases with the decrease of freezing temperature.

Fig. 10. Critical stress intensity factors calculated at different (a) flaw inclination angles and (b) freezing temperatures.
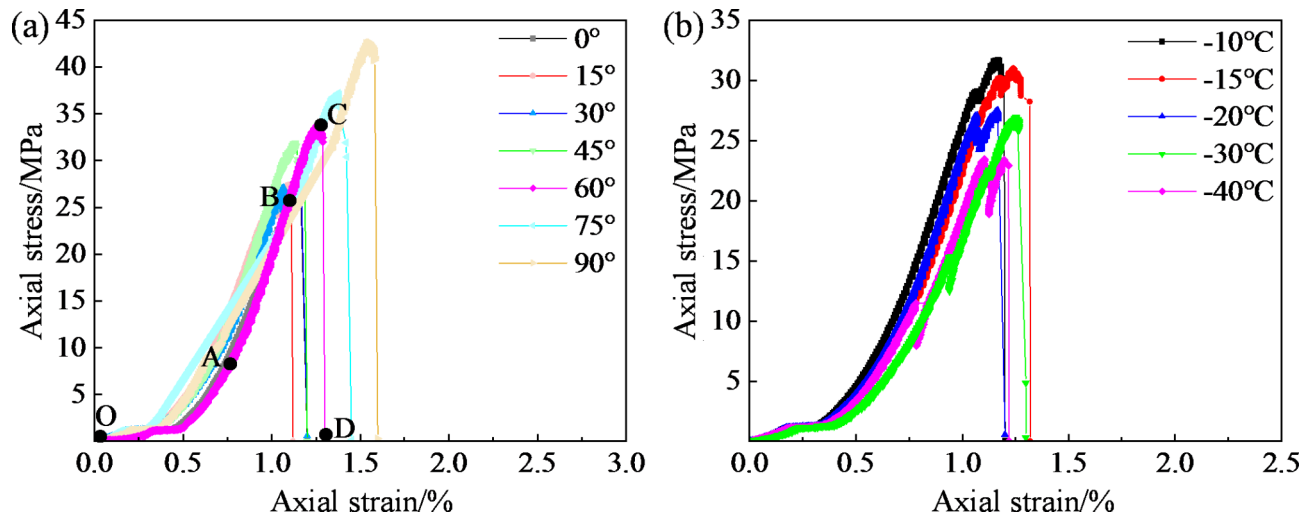
Fig. 11. Uniaxial compression stress–strain curves of melted samples after frost heave cracking at different (a) flaw inclination angles and (b) freezing temperatures.
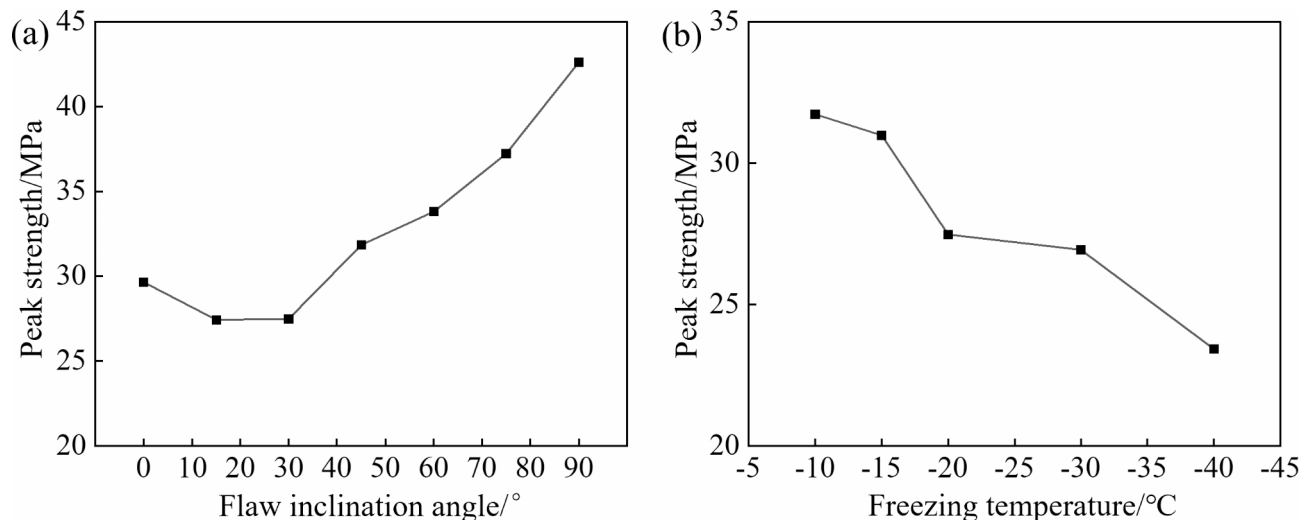
Fig. 12. Uniaxial compression strengths of melted samples after frost heave cracking at different (**a**) flaw inclination angles and (**b**) freezing temperatures.

Plastic deformation stage (BC): With the increase of compression load, prefabricated flaw or frost heave-induced cracks begin to extend, and the curve may fluctuate, but it can still withstand compression stress until the peak stress state.

Failure stage (CD): After the peak stress, some cracks quickly penetrate the sample, the sample fails and loses the load-bearing capacity, and the stress falls rapidly.

Uniaxial compression strength
Figure 12 displays the variation of uniaxial compressive strength of melted samples after frost heave cracking at different flaw inclination angles and freezing temperatures. As can be seen from Fig. 12a, with the increase of flaw inclination angle, the uniaxial compression strength first decreases and then increases, and is the smallest when the flaw inclination angle is in the range of 10 ~ 30° and the largest when the flaw inclination angle is 90°. Specifically, from the inclination angle of 0° to 30°, the uniaxial compression strength decreases from 29.73 MPa to 27.48 MPa, a decrease of 7.57%, which is relatively small. From the inclination angle of 30° to 90°, the uniaxial compression strength increases significantly from 27.48 MPa to 42.64 MPa, an increase of 55.17%. As can be seen from Fig. 12b, the uniaxial compression strength decreases with the drop of freezing temperature. The freezing temperature is reduced from −10 °C to −40 °C, the uniaxial compression strength is reduced from 31.73 MPa to 23.43 MPa, and the reduction rate is 0.28 MPa/°C.

Cracking mode of flaw

Effect of flaw inclination angle on cracking mode

Figure 13 exhibits the uniaxial compression failure mode of melted samples with different flaw inclination angles after frost heave cracking at freezing temperature of -20 °C. The red lines in the figure represent the cracks caused by frost heave, and the blue lines represent the cracks caused by uniaxial compression.

When the flaw inclination angle is 0°, wing cracks T_1 and T_2 and shear crack S initiate at the flaw ends. The wing crack T_2 at the upper end of the flaw is connected with crack S. In addition, a tensile crack T_3 initiates on the upper surface of the flaw and joins with the wing crack T_2. Frost heave-induced cracks have no effect on the cracks caused by uniaxial compression. When the flaw inclination angle is 15°, similar to flaw inclination angle of 0°, wing cracks T_1 and T_2 and shear crack S mainly initiate at the flaw ends. Frost heave-induced cracks have little effect on the cracks caused by uniaxial compression. When the flaw inclination angle is 30°, wing cracks T_1 and T_2 initiate at the flaw ends and extend along the loading direction, but stop after a certain length of extending, while the developed shear cracks S_1 and S_2 penetrate the sample. Frost heave-induced cracks have little effect on the cracks caused by uniaxial compression. When the flaw inclination angle is 45°, coplanar shear cracks S_1 and S_2 initiate from the flaw ends and penetrate the sample, and shear failure occurs in the whole sample. The cracks caused by uniaxial compression are affected by frost heave-induced cracks and have a certain overlap with frost heave-induced cracks. When the flaw inclination angle is 60°, coplanar shear cracks S_1 and S_2 initiate at the tips of the frost heave-induced cracks and penetrate the sample. In addition, a wing crack T develops and deflects at the left end of the flaw. Finally, shear failure occurs on the whole sample. Frost heave-induced cracks have great influence on the cracks caused by uniaxial compression. When the flaw inclination angle is 75°, coplanar shear cracks S_1 and S_2 initiate at the tips of the frost heave-induced cracks and turn to the loading direction, finally penetrating the sample. In addition, a shear crack S_3 is partially outlaid in the upper shear crack S_2. Frost heave-induced cracks have great influence on the cracks caused by uniaxial compression. When the flaw inclination angle is 90°, four shear cracks develops from the middle of the flaw, forming two conjugate shear fracture planes in general. Frost heave-induced cracks have no effect on the cracks caused by uniaxial compression.

The above analysis illustrates that when the flaw is in a certain inclination angle range, the frost heave-induced cracks have an effect on the crack path generated by uniaxial compression, while when the flaw inclination angle is small or large, the frost heave-induced cracks have no effect on the crack path generated by uniaxial compression.

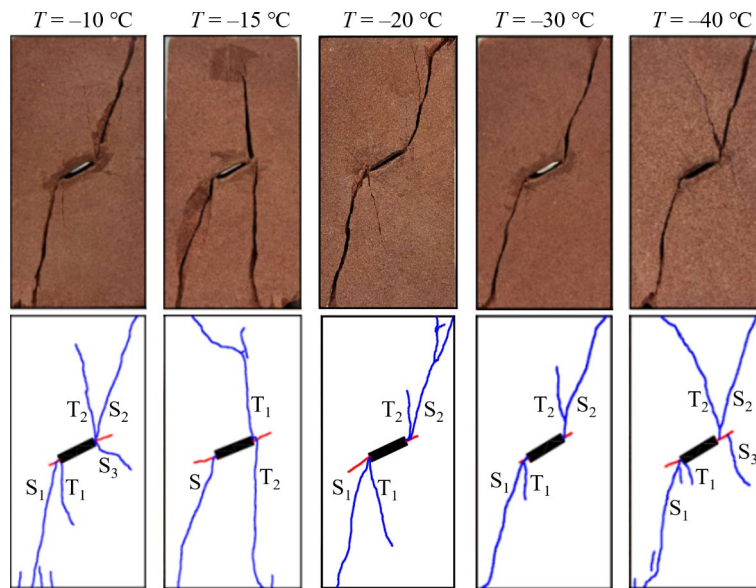### *Effect of freezing temperature on cracking mode*

Figure 14 shows the uniaxial compression failure mode of melted samples with 30° flaw inclination angle after frost heave cracking at different freezing temperatures. When the freezing temperature is -10 °C, wing cracks T_1 and T_2 and shear cracks S_1, S_2 and S_3 initiate at the ends of the flaw, but shear cracks S_1 and S_2 mainly cause shear through failure in the sample. When the freezing temperature is -15 °C, wing crack T_1 and anti-wing crack T_2 initiate at the right end of the flaw, and shear crack S initiates at the left end of the flaw, and the sample as a whole shows tensile–shear mixed failure. When the freezing temperature is -20 °C, wing cracks T_1 and T_2 and shear cracks S_1 and S_2 initiate at the ends of the flaw, but shear cracks S_1 and S_2 mainly cause shear through failure in the sample. When the freezing temperature is -30 °C, the cracks develop are similar to those at -20 °C. When the freezing temperature is -40 °C, the cracks develop are similar to those at -10 °C. In general, frost heave-induced cracks of 30° flaw inclination angle at different freezing temperatures have little effect on cracks caused by uniaxial compression.

Conclusions

Low temperature frost heave test and uniaxial compression test after frost heave on water-filled single-flaw sandstone samples were carried out, and the flaw frost heave cracking mode, frost heave pressure, frost heave
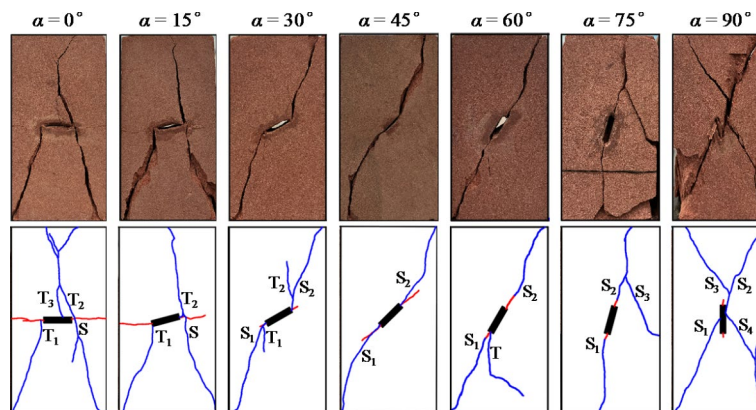
Fig. 13. Uniaxial compression failure mode of melted samples with different flaw inclination angles after frost heave cracking at freezing temperature of -20 °C (the red lines represent the cracks caused by frost heave and the blue lines represent the cracks caused by uniaxial compression).

Fig. 14. Uniaxial compression failure mode of melted samples with 30° flaw inclination angle after frost heave cracking at different freezing temperatures (the red lines represent the cracks caused by frost heave and the blue lines represent the cracks caused by uniaxial compression).

cracking criterion and the effect of frost heave-induced cracks on uniaxial compression failure behavior under different flaw inclination angles and freezing temperatures were investigated. The conclusions are as follows:

(1) Cracks initiate and extend along the coplanar direction of flaws under the action of frost heave in general, and the frost heave damage degree decreases with the increase of flaw inclination angle. As the freezing temperature drops, the crack propagation length first increases greatly, and then decreases, reaching the maximum at − 15 ℃.

(2) The evolution of frost heave pressure in the flaw can be divided into six stages: Pre-freezing stage (temperature has not yet dropped to 0 ℃, frost heave pressure is zero), rapid increase stage (temperature reaches freezing point 0 ℃, water–ice phase transition), rapid decrease stage (cracking of flaw), stable stage (freezing temperature constant stage), slight rebound stage (temperature rises, rock matrix cold shrinkage rebound and squeeze the ice in the flaw), dissipation stage (temperature rises to above 0 ℃, ice melts).

(3) The peak frost heave pressure first increases and then decreases with the increase of flaw inclination angle, and reaches the maximum when the flaw inclination angle is 60°. It increases as the freezing temperature drops. Based on fracture mechanics theory and peak frost heave pressure test data, the critical stress intensity factor (K_{IC}) formula for flaw cracking under frost heave pressure is given. The calculated results were fitted to obtain the frost heave cracking criterion considering the flaw inclination angle or freezing temperature.

(4) The flaw inclination angle and freezing temperature have influence on the uniaxial compression stress–strain curves of the samples after frost heave. The uniaxial compression strength of the samples after frost heave first decreases and then increases with the increase of the flaw inclination angle, and is the smallest when the flaw inclination angle ranges from 10° to 30° and the largest when the flaw inclination angle is 90°. The uniaxial compression strength decreases as the freezing temperature drops.

(5) When the flaw is in a certain inclination angle range (45 ~ 75°), cracks under uniaxial compression will extend from the frost heave-induced cracks, that is, frost heave-induced cracks will affect the crack path generated by uniaxial compression. The frost heave-induced cracks of samples with 30° flaw inclination angle at different freezing temperatures have almost no effect on the crack path generated by uniaxial compression.

It should be noted that in this study only one type of rock was tested, considering only one freezing temperature (–20 ℃) when analyzing the effect of flaw inclination angle, and only one flaw inclination angle (30°) when analyzing the effect of freezing temperature (–10~–40 ℃). Therefore, the applicability of some conclusions in this paper outside of these conditions requires further investigation.

Data availability
The data used to support the findings and results of this study are available from the corresponding author upon request.

References

1. Michaud, Y. & Dyke, L. D. Mechanism of bedrock frost heave in permafrost regions. Pergélisol–Canada, actes de la Cinquième conférence canadienne sur le pergélisol, conseil national de recherches Canada et Centre d'études nordiques. *Laval Italia: Université Laval.* **54**, 125–130 (1990).
2. Huang, S., Liu, Q., Cheng, A. & Liu, Y. A statistical damage constitutive model under freeze–thaw and loading for rock and its engineering application. *Cold Reg. Sci. Technol.* **145**, 142–150 (2018).
3. Xia, C., Lv, Z., Li, Q., Huang, J. & Bai, X. Transversely isotropic frost heave of saturated rock under unidirectional freezing condition and induced frost heaving force in cold region tunnels. *Cold Reg. Sci. Technol.* **152**, 48–58 (2018).
4. Zhang, C. et al. An elasto-visco-plastic model based on stress functions for deformation and damage of water-saturated rocks during the freeze–thaw process. *Constr. Build. Mater.* **250**, 118862 (2020).
5. Li, Q., Li, Q., Wang, F., Wu, J. & Wang, Y. The carrying behavior of water-based fracturing fluid in shale reservoir fractures and molecular dynamics of sand-carrying mechanism. *Processes* 12 (2024). (2051).
6. Li, Q., Li, Q. & Han, Y. A numerical investigation on kick control with the displacement kill method during a well test in a deep-water gas reservoir: A case study. *Processes* 12 (2024). (2090).
7. Winkler, E. M. Frost damage to stone and concrete: Geological considerations. *Eng. Geol.* **2**(5), 315–323 (1968).
8. Davidson, G. P. & Nye, J. F. A photoelastic study of ice pressure in rock cracks. *Cold Reg. Sci. Technol.* **11**(2), 141–153 (1985).
9. Arosio, D., Longoni, L., Mazza, F., Papini, M. & Zanzi, L. *Freeze–Thaw Cycle and Rockfall Monitoring. Landslide Science and Practice* (Springer, 2013).
10. Huang, S., Wang, J., Liu, Y., Tian, Q. & Cai, C. Experimental investigation on crack coalescence and strength loss of rock-like materials containing two parallel water-filled flaws under freeze–thaw. *Teor Appl. Fract. Mech.* **123**, 103669 (2023).
11. Lin, H., Lei, D., Zhang, C., Wang, Y. & Zhao, Y. Deterioration of non-persistent rock joints: A focus on impact of freeze–thaw cycles. *Int. J. Rock. Mech. Min.* **135**, 104515 (2020).
12. Liu, L. et al. Modeling of the internal damage of saturated cement paste due to ice crystallization pressure during freezing. *Cem. Concrete Comp.* **33**(5), 562–571 (2011).
13. McGreevy, J. P. & Whalley, W. B. Rock moisture content and frost weathering under natural and experimental conditions: A comparative discussion. *Arct. Antarct. Alp. Res.* **17**(3), 337–346 (1985).
14. Derjaguin, B. V. & Churaev, N. V. Flow of nonfreezing water interlayers and frost heaving. *Cold Reg. Sci. Technol.* **12**(1), 57–66 (1986).
15. Churaev, N. V. & Sobolev, V. D. Disjoining pressure of thin unfreezing water layers between the pore walls and ice in porous bodies. *Colloid J. +.* **64**(4), 508–511 (2002).
16. Vlahou, I. & Worster, M. G. Ice growth in a spherical cavity of a porous medium. *J. Glaciol.* **56**(196), 271–277 (2010).
17. Walder, J. & Hallet, B. A theoretical model of the fracture of rock during freezing. *Geol. Soc. Am. Bull.* **96**(3), 336–346 (1985).
18. Tan, X., Chen, W., Tian, H. & Cao, J. Water flow and heat transport including ice/water phase change in porous media: Numerical simulation and application. *Cold Reg. Sci. Technol.* **68**(1–2), 74–84 (2011).
19. Tan, X., Chen, W., Yang, J. & Cao, J. Laboratory investigations on the mechanical properties degradation of granite under freeze–thaw cycles. *Cold Reg. Sci. Technol.* **68**(3), 130–138 (2011).
20. Murton, J. B. et al. Experimental design for a pilot study on bedrock weathering near the permafrost table. *Earth Surf. Proc. Land.* **25**(12), 1281–1294 (2000).
21. Murton, J. B., Peterson, R. & Ozouf, J. C. Bedrock fracture by ice segregation in cold regions. *Science* **314**(5802), 1127–1129 (2006).
22. Liu, H., Yuan, X. & Xie, T. A damage model for frost heaving pressure in circular rock tunnel under freezing–thawing cycles. *Tunn. Undergr. Sp Tech.* **83**, 401–408 (2019).
23. Jia, H., Leith, K. & Krautblatter, M. Path dependent frost wedging experiments in fractured, low permeability granite. *Permafr. Periglac.* **28**(4), 698–709 (2017).
24. Lv, Z., Xia, C., Wang, Y. & Lin, Z. Frost heave and freezing processes of saturated rock with an open crack under different freezing conditions. *Front. Struct. Civ. Eng.* **14**(4), 947–960 (2020).
25. Tharp, T. M. Conditions for crack propagation by frost wedging. *Geol. Soc. Am. Bull.* **99**(1), 94–102 (1987).
26. Jia, H. L., Han, L., Zhao, T., Sun, Q. & Tan, X. J. Strength and the cracking behavior of frozen sandstone containing ice-filled flaws under uniaxial compression. *Permafr. Periglac.* **33**(2), 160–175 (2022).
27. Liu, W., Han, L., Wu, D., Jia, H. & Tang, L. Variability in mechanical properties and cracking behavior of frozen sandstone containing en echelon flaws under compression. *Appl. Sci. Basel.* **14**(8), 3427 (2024).
28. Wang, T. et al. Failure behaviour of frozen rock with double ice-filled flaws under Brazilian splitting tension. *Eng. Fract. Mech.* **304**, 110124 (2024).
29. Bai, Y. et al. Experimental study on the strength, deformation and crack evolution behaviour of red sandstone samples containing two ice-filled fissures under triaxial compression. *Cold Reg. Sci. Technol.* **174**, 103061 (2020).
30. Huang, S., Liu, Y., Guo, Y., Zhang, Z. & Cai, Y. Strength and failure characteristics of rock-like material containing single crack under freeze–thaw and uniaxial compression. *Cold Reg. Sci. Technol.* **162**, 1–10 (2019).
31. Shan, R. L. et al. Study on the triaxial unloading creep mechanical properties and damage constitutive model of red sandstone containing a single ice-filled flaw. *Rock. Mech. Rock. Eng.* **54**(2), 833–855 (2021).
32. Zhu, C. et al. Investigation on the dynamic cracking mechanism of sandstone with an ice-saturated flaw based on drop weight tests. *Rock. Mech. Rock. Eng.* (2024).
33. Huang, S. et al. Frost heaving and frost cracking of elliptical cavities (fractures) in low-permeability rock. *Eng. Geol.* **234**, 1–10 (2018).

Acknowledgements

Author contributions

D. C. designed the research and wrote the main manuscript. Y.L. conducted the tests and data processing.

Declarations

Competing interests

The authors declare no competing interests.

Additional information

Correspondence and requests for materials should be addressed to D.C.

Reprints and permissions information is available at www.nature.com/reprints.